

April 2025

Critical Behaviour in the Single Flavor Thirring Model in 2+1d with Wilson Kernel Domain Wall Fermions

Simon Hands^a and Jude Worthy^b

^b *Department of Mathematical Sciences, University of Liverpool,
Liverpool L69 3BX, United Kingdom.*

^b *Department of Physics, College of Science, Swansea University,
Singleton Park, Swansea SA2 8PP, United Kingdom.*

Abstract: We present results of a lattice field theory simulation of the 2+1d Thirring model with $N = 1$ fermion flavors, using domain wall fermions. The model exhibits a U(2) symmetry-breaking phase transition with the potential to define a UV-stable renormalisation group fixed point. The novelty is the replacement of the Shamir kernel used in all previous work with the Wilson kernel, improving the action particularly with respect to the $L_s \rightarrow \infty$ limit needed to recover U(2), now under much better control. Auxiliary field ensembles generated on $16^3 \times 24$ with varying self-interaction strength g^2 and bare mass m are used to measure the bilinear condensate order parameter $\langle \bar{\psi} i\gamma_5 \psi \rangle$ with domain wall separations as large as $L_s = 120$. The resulting $L_s \rightarrow \infty$ extrapolation is used to fit an empirical equation of state modelling spontaneous symmetry breaking as $m \rightarrow 0$. The fit is remarkably stable and compelling, with the fitted critical exponents $\beta_m \simeq 2.4$, $\delta \simeq 1.3$ differing markedly from previous estimates. The associated susceptibility exhibits a mass hierarchy in line with physical expectations, again unlike previous estimates. Schwinger-Dyson equation (SDE) solutions of the Thirring model exploiting a hidden local symmetry in the action are reviewed, and analytic predictions presented for the exponents. In contrast to all previous lattice studies, the universal characteristics of the critical point revealed qualitatively resemble the SDE predictions.

Keywords: Lattice Gauge Field Theories, Field Theories in Lower Dimensions, Global Symmetries

1 Introduction

The $2+1d$ Thirring model describes relativistic fermions interacting via a local contact term between conserved currents, with continuum Lagrangian density

$$\mathcal{L}_{\text{cont}} = \sum_{i=1}^N \bar{\psi}_i (\not{d} + m) \psi_i + \frac{g^2}{2N} \sum_i (\bar{\psi}_i \gamma_\mu \psi_i)^2. \quad (1)$$

Here N is the number of flavors each described by a 4-component spinor. Since there are two Dirac matrices γ_3, γ_5 which anti-commute with the kinetic term, for $m = 0$ (1) has a symmetry under $U(2N)$ global flavor rotations which is broken to $U(N) \otimes U(N)$ by a bilinear mass term such as $\bar{\psi}\psi, i\bar{\psi}\gamma_{3,5}\psi$. For sufficiently strong interaction strength this breaking can occur spontaneously, and it is believed that at fixed N the coupling g_c^2 marks a UV-stable renormalisation group fixed point where an interacting continuum limit may be found.

As further elaborated in Sec. 4 below, since small values of N are expected to be the most important and accordingly *a priori* no small parameter available, non-perturbative methods are mandatory when studying the symmetry-breaking dynamics. Analytic approaches applied include Schwinger-Dyson equations (SDE) [1, 2, 3, 4] and Functional Renormalisation Group (FRG) [5, 6, 7]. There have also been several approaches based on numerical simulation of lattice field theory – see [8] for a recent review. Interest in the problem has been renewed with the realisation that for a strongly-coupled problem the lattice formulation should ideally faithfully respect the correct $U(2N)$ symmetry at a microscopic level, leading to recent studies using both Domain Wall (DWF) and SLAC fermions [9].

The DWF approach has been explored in a series of papers [10, 11, 12, 13]. In order to recover $U(2N)$ it is necessary to take the limit $L_s \rightarrow \infty$ where L_s is the separation of the domain walls in a fictitious “third” direction x_3 . While the nature of the limit is quite well understood [14, 15], achieving it with sufficient numerical control has proved challenging, in part because the lattice formulation to be reviewed in Sec. 2 below employs non-unitary link fields $1+iA_\mu$ making the fermion matrix $D_{\text{DWF}}[A]$ rather ill-conditioned. Recent attempts with $N = 1$ and $L_s \leq 48$ found evidence that while $U(2)$ is recovered only rather slowly as $L_s \rightarrow \infty$ it is indeed spontaneously broken at sufficiently strong coupling, implying that the critical N_c above which the symmetry is unbroken at all couplings is bounded by $N_c > 1$. The associated equation of state (EoS, specified in (11) below) in the vicinity of the transition is characterised by two critical exponents $\beta_m \approx 0.3, \delta \approx 4$ [11, 12].

In this paper we apply an improved DWF operator to the problem, replacing the previously-used Shamir kernel $\gamma_3 D_W (2 + D_W)^{-1}$ of the associated $2+1d$ overlap operator D_{ov} with the better-behaved Wilson kernel $\gamma_3 D_W$. Operationally, this is implemented by altering the definition of the derivative in the third direction in the DWF operator, as described in Sec. 2 below. Details of the algorithm are set out in [16]. The Wilson kernel’s eigenvalue spectrum is bounded from above, and pilot studies [17, 16] show it

to be much better conditioned than the Shamir kernel in the symmetry broken phase, at the cost of slightly lower RHMC acceptance. It also gives superior convergence to $U(2N)$ -symmetry as $L_s \rightarrow \infty$, as measured by the residual in the Ginsparg-Wilson relation [12].

In this paper we restrict attention to the model with $N = 1$. By studying the order parameter $\langle \bar{\psi} \psi(g^2, m) \rangle$ on spacetime volume 16^3 extrapolated to $L_s \rightarrow \infty$ we have found the Wilson kernel formulation yields a more compelling fit to an empirical critical EoS than obtained previously, with significant impact on the critical parameters. The critical coupling g_c^2 is shifted to a much weaker value than the estimate of [12], and the exponents modified to $\beta_m \gtrsim 2$, $\delta \approx 1.3$. The emerging picture of criticality is much more similar to the predictions of SDE [4] than that suggested by any previous lattice study.

The rest of the paper is organised as follows. Sec. 2 reviews the definition of the lattice Thirring model with DWF, which employs a bosonic auxiliary field A_μ defined on the links of the spacetime lattice, and outlines the simulation methods. Numerical results are presented in Sec. 3, including: details of the L_s extrapolation of condensate measurements made on ensembles $\{A_\mu\}$ generated at fixed L_s ; the impact of varying L_s in the ensemble generation; fits to the resulting EoS to extract critical parameters; and the associated order parameter susceptibility $\chi_\ell = \partial \langle \bar{\psi} \psi \rangle / \partial m$. Pointers to previous results obtained using Shamir kernel are given for comparison: the Wilson kernel yields a more robust extrapolation and the EoS fit is remarkably stable. Moreover in contrast to previous findings χ_ℓ increases as $m \rightarrow 0$, matching expectations based on the EoS. In Sec. 4 we change tack, reviewing a description of Thirring criticality based on solving SDEs, using an approach which exploits a hidden local symmetry in (1) to predict $N_c \simeq 4.32$. However, the limits $N \rightarrow N_c$ and $g^2 \rightarrow g_c^2$ are found not to commute; since $\langle \bar{\psi} \psi \rangle$ should be a function of state this suggests this analysis is not complete. Much of this material already exists in the literature [2, 4], but here special attention is paid to deriving critical exponents. Finally Sec. 5 discusses the numerical results in this context, and speculates on the N -dependence of the universal scaling at the fixed points with $N < N_c$.

2 Formulation & Methodology

Fermion fields $\Psi(x, s), \bar{\Psi}(x, s)$ with four spinor components are defined on the sites of an $L^3 \times L_s$ lattice, where L^3 determines the spacetime volume and L_s the domain wall separation, via the bilinear form

$$\begin{aligned} \bar{\Psi} D_{DWF} \Psi &\equiv \sum_{x,y} \sum_{s,s'} \bar{\Psi}(x, s) \left[\delta_{s,s'} D_{Wx,y}[A] + D_{3x,y;s,s'}[A] \right] \Psi(y, s') \\ &+ im \sum_{x,y} \left(-\bar{\Psi}(x, L_s) (1 - D_W)_{x,y} P_- \Psi(y, 1) + \bar{\Psi}(x, 1) (1 - D_W)_{x,y} P_+ \Psi(y, L_s) \right), \end{aligned} \quad (2)$$

where m is the bare mass, $P_{\pm} = \frac{1}{2}(1 \pm \gamma_3)$,

$$D_{Wx,y}[A] \equiv -\frac{1}{2} \sum_{\mu=0,1,2} \left[(1-\gamma_{\mu})(1+iA_{\mu}(x))\delta_{x+\hat{\mu},y} + (1+\gamma_{\mu})(1-iA_{\mu}(x))\delta_{x-\hat{\mu},y} \right] + (3-M)\delta_{x,y}, \quad (3)$$

with M the domain wall height, and

$$D_{3x,y;s,s'}[A] = \left[(D_{Wx,y}[A]-1)P_{-}\delta_{s+1,s'}(1-\delta_{s',L_s}) + (D_{Wx,y}[A]-1)P_{+}\delta_{s-1,s'}(1-\delta_{s',1}) \right] + \delta_{s,s'}. \quad (4)$$

Here $A_{\mu}(x)$ is a real three-dimensional auxiliary boson field defined on the link between x and $x + \hat{\mu}$, whose fluctuations are moderated by the gaussian form $S_{\text{bose}} = \sum_{x,\mu} A_{\mu}^2(x)/2g^2$. Integration over A yields four-fermi interactions expressible as a contact interaction between conserved but non-local fermion currents [13] depending on $\Psi, \bar{\Psi}$ throughout the bulk. The model is completed by specifying fields $\psi, \bar{\psi}$ living in the Thirring model's 2+1d target space in terms of $\Psi, \bar{\Psi}$ on the domain walls:

$$\psi(x) = P_{-}\Psi(x, 1) + P_{+}\Psi(x, L_s); \quad \bar{\psi}(x) = \bar{\Psi}(y, L_s)(1 - D_W)_{y,x}P_{-} + \bar{\Psi}(y, 1)(1 - D_W)_{y,x}P_{+}, \quad (5)$$

whence the mass term in (3) is seen to be equivalent to $im\bar{\psi}\gamma_3\psi$.

A key property of the Wilson operator is its γ_3 -hermiticity $\gamma_3 D_W \gamma_3 = D_W^{\dagger}$. In the large- L_s limit it is possible to show [15] that D_{DWF} is equivalent to the 2+1d overlap operator¹

$$D_{\text{ov}} = \frac{1}{2} \left[(1 + im\gamma_3) + \frac{D_W}{\sqrt{D_W^{\dagger} D_W}}(1 - im\gamma_3) \right], \quad (6)$$

in which case the U(2) symmetry of the continuum Thirring model is realised in the Ginsparg-Wilson sense. The appearance of $\text{sgn}(\gamma_3 D_W)$ in (6) underlies the designation “Wilson kernel”. The equivalence holds in the sense that $\lim_{L_s \rightarrow \infty} \det[D_{DWFh}^{-1}(m=1)D_{DWF}(m)] = \det D_{\text{ov}}(m)$, where for D_{DWHh} the antihermitian mass term in (3) is replaced by the more familiar hermitian $m\bar{\psi}\psi$ [15].

Monte Carlo simulations of the model were performed on a $16^3 \times L_s$ lattice using the RHMC algorithm set out in [11, 12], with domain wall height $Ma = 1$, but with the Shamir kernel employed in those studies replaced by the Wilson kernel (4) as described in [16]. Initially auxiliary field ensembles were generated with $L_s = 24$, which were then used to estimate the bilinear order parameter for U(2) symmetry breaking $i\langle\bar{\psi}\gamma_3\psi\rangle$ using $L_s = 24, 32, 48, 72, 96$ and 120 , chosen to facilitate the $L_s \rightarrow \infty$ extrapolation. The bilinear was estimated on each configuration using 10 independent gaussian noise vectors for each of the components $-\bar{\Psi}(L_s)(1 - D_W)P_{-}\Psi(1), \bar{\Psi}(1)(1 - D_W)P_{+}\Psi(L_s)$. The required matrix inversions were performed using a conjugate gradient routine with stopping residual 10^{-5} per vector element. The non-compact nature of the auxiliary A_{μ} makes the inversion numerically challenging; the number of CG iterations required for

¹For L_s finite Wilson-kernel D_{DWF} is equivalent to a truncated overlap operator.

measurement on $L_s = 24(120)$ rises from ~ 4500 (~ 5500) at the weakest coupling g^2 and largest fermion mass m explored to ~ 12000 (~ 14000) at the strongest coupling and smallest mass. Over the same parameter range the RHMC acceptance rate on $L_s = 24$ varied from $\sim 82\%$ to $\sim 65\%$.

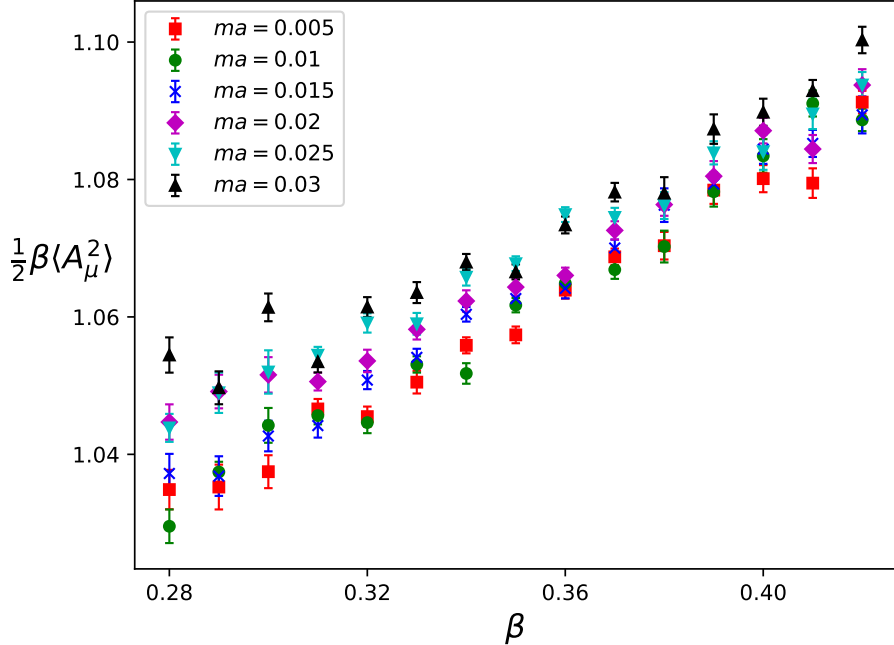


Figure 1: Auxiliary boson action density vs. coupling β from RHMC production runs on $16^3 \times 24$, averaged using a binsize of 20 to mitigate autocorrelations.

Pilot studies using the Wilson kernel action on a 12^3 spacetime lattice [17, 16] suggest a U(2) symmetry breaking transition in the region $\beta \sim 0.30 - 0.35$, where the dimensionless coupling $\beta \equiv ag^{-2}$. Accordingly we generated a total of 90 auxiliary ensembles with $\beta \in [0.28, 0.29, \dots, 0.42]$ and bare mass $ma \in [0.005, 0.01, \dots, 0.03]$. Configurations were stored following every 5 RHMC trajectories, with random trajectory length drawn from a Poisson distribution with mean length 1.0; in all cases at least 100 configurations were generated for each parameter set, with 300 configurations generated for the region $\beta \in [0.31, 0.37]$ where, based on visual inspection of the $L_s = 24$ data, the order parameter fluctuations were largest.

Fig. 1 shows the boson action density estimated over the entire parameter set. With admittedly large statistical fluctuations, this quantity appears to vary smoothly and evenly within the confines of the parameter range explored. Similarly to what was found for the bulk formulation with Shamir kernel, interaction with the fermions reduces S_{bose} below its non-interacting value $S_{\text{bose}}^{\text{free}} = \frac{3}{2}$, the effect increasing as $m \rightarrow 0$. Compared to Shamir kernel the departure from free-field behaviour is significantly enhanced, as can be

seen by comparison with Fig. 13 of [12]. There is no sign of the non-monotonic behaviour seen in that study, which hinted at complicated behaviour in the strong-coupling limit. It is also striking that within the critical region identified in studies using the Shamir kernel S_{bose} is a *decreasing* function of β , in contrast to the behaviour shown in Fig. 1. The physical interpretation of S_{bose} in the bulk formulation is not transparent [11], and it is clear far greater statistics would be needed to obtain it with precision. The effect of generating the auxiliary ensemble with $L_s > 24$ will be addressed below.

3 Results & Analysis

3.1 Extrapolation $L_s \rightarrow \infty$

Our strategy is a partially-quenched one:² we approach the limit $L_s \rightarrow \infty$ by performing measurements in the valence sector for $L_s = 24, \dots, 120$. First, in order to assess U(2) symmetry recovery in this limit we define a residual δ_h :

$$\delta_h(L_s) = \frac{1}{2} \text{Im} \langle \bar{\Psi}(1)(1 - D_W)P_+ \Psi(L_s) + \bar{\Psi}(L_s)(1 - D_W)P_- \Psi(1) \rangle. \quad (7)$$

In [14] it was demonstrated that δ_h is an effective proxy³ for the splitting between

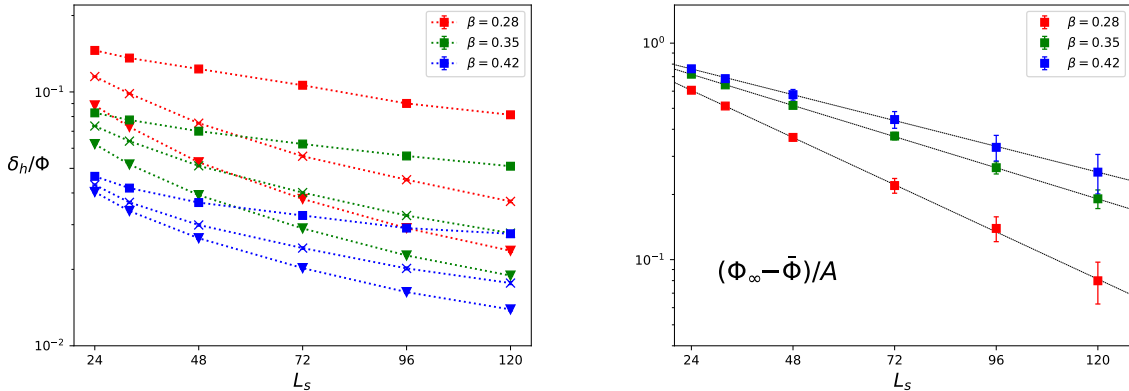


Figure 2: (Left) Ratio of the residual $\delta_h(L_s)$ to the condensate $\Phi(L_s)$ plotted on a log scale for three representative couplings and $ma = 0.005$ (\square), 0.015 (\times), 0.025 (∇)); (Right) $(\Phi_\infty - \bar{\Phi})/A$ vs. L_s on the same scale for the same three couplings at $ma = 0.005$, together with a fit to (8).

the condensates $\langle \bar{\psi}\psi \rangle$ and $i\langle \bar{\psi}\gamma_3\psi \rangle, i\langle \bar{\psi}\gamma_5\psi \rangle$, which must vanish in a U(2)-symmetric theory. The left panel of Fig. 2 shows δ_h/Φ (where Φ stands as a shorthand for the order parameter $i\langle \bar{\psi}\gamma_3\psi \rangle$) as a function of L_s for three representative couplings. The

²The optimised DWF studied in [17, 16] which use an improved approximation to the signum function in (6) were found to be prohibitively expensive on the spacetime volume used in this study.

³At least in a model where the bose fields vary smoothly and compactly, such as QED₃.

data fall in three groups, ranked in decreasing magnitude as the mass ma increases. The ratio falls monotonically consistent with U(2) restoration in the $L_s \rightarrow \infty$ limit, but Fig. 2 suggests the decay is slower than exponential. In fact, replotted with log scales on both axes suggests the decay is also faster than a power law. We deduce that for this parameter set and range of accessible L_s the residual δ_h has a mild coupling dependence and is governed by more than one, indeed possibly several, scale(s). Corresponding data obtained with the Shamir kernel is shown in Fig. 12 of [11].

Using measurements taken on N_{L_s} different L_s with independent noisy sources, we extrapolate results to the $L_s \rightarrow \infty$ limit using an exponential *Ansatz* [11]:

$$\Phi(L_s) = \Phi_\infty - A \exp(-\Delta L_s), \quad (8)$$

where fit parameters A , Δ and Φ_∞ all depend on m and β . Since $\Phi(L_s)$ data are taken on the same underlying auxiliary field ensembles, the fit takes correlations into account by minimising $\chi^2 = (\Phi^{\text{fit}} - \bar{\Phi})C^{-1}(\Phi^{\text{fit}} - \bar{\Phi})$ where $\Phi^{\text{fit}}(L_s; \Phi_\infty, A, \Delta)$ is given by (8), $\bar{\Phi}$ denotes the average over the dataset at fixed L_s and the $N_{L_s} \times N_{L_s}$ covariance matrix is

$$C_{L_{s1}, L_{s2}} = \frac{1}{N_{\text{dat}}(N_{\text{dat}} - 1)} \sum_{i=1}^{N_{\text{dat}}} (\Phi_{i, L_{s1}} - \bar{\Phi}_{L_{s1}})(\Phi_{i, L_{s2}} - \bar{\Phi}_{L_{s2}}). \quad (9)$$

The right panel of Fig. 2 compares the fit with data for three representative couplings

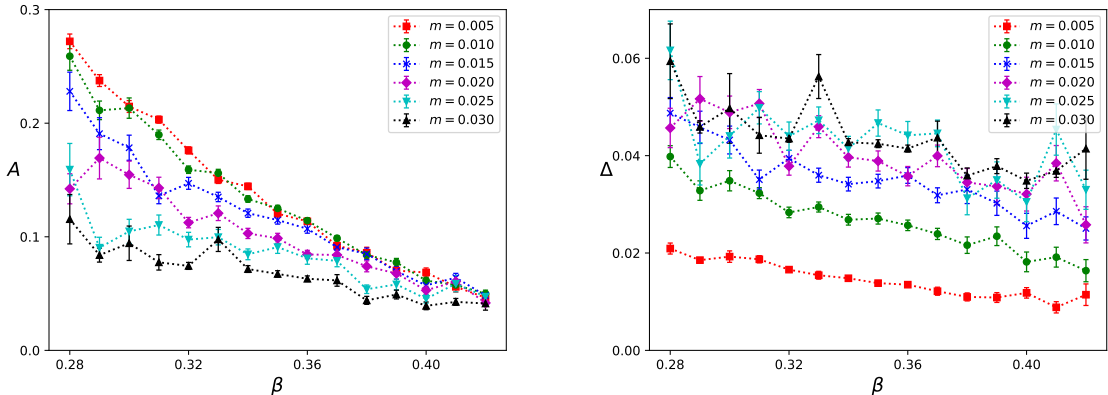


Figure 3: Fit parameters A (left panel) and Δ (right) resulting from the exponential Ansatz (8) applied to $L_s \in \{24, 32, 48, 72, 96, 120\}$.

at $ma = 0.005$, and Fig. 3 shows the fit parameters extracted using data from 6 values of $L_s \in [24, 120]$. The average χ^2 per degree of freedom over the 90 parameter sets is 2.15, with no value exceeding 6 save for one outlier at $\beta = 0.31, ma = 0.02$ (which does not stand out in Fig. 3). Below we shall explore the consequences of removing some data from the fit. Within fluctuations which increase as A decreases and/or Δ increases (so the overall extrapolation decreases in magnitude), the plots show a regular

behaviour as functions of both β and m . It is interesting that the fit quality improves as the extrapolation becomes numerically more important, ie. at small mass and strong coupling. A comparable analysis for the Shamir kernel is shown in Fig. 2 of [12].

L_s (sea)	S_{bose}	$\bar{\Phi}_{24}$	$\bar{\Phi}_{32}$	$\bar{\Phi}_{120}$	Φ_∞
24	1.0553(12)	0.0814(8)	0.0916(10)	0.1582(24)	0.1821(25)
32	1.0569(12)	0.0798(8)	0.0905(11)	0.1480(21)	0.1644(31)

Table 1: Comparison of ensembles generated with varying L_s at $\beta = 0.34$, $ma = 0.005$.

It is important to quantify the uncontrolled and non-unitary approximation made by taking $L_s(\text{sea}) \neq L_s(\text{valence})$, assumed in our analysis to make negligible difference. Table 1 compares the reference ensemble at $\beta = 0.34$, $ma = 0.005$ generated with $L_s = 24$ and a similar-sized one generated with $L_s = 32$. The values for the auxiliary boson action S_{bose} are compatible, but higher-order correlations may still be important. We follow the same analysis procedure, measuring the sequence $\bar{\Phi}_{L_s}$ and then extrapolating to determine Φ_∞ . For $L_s(\text{valence}) = 24, 32$ the results are compatible, but by $L_s = 120$ a small but significant difference is present, resulting in $\Phi_\infty^{32} < \Phi_\infty^{24}$. With present resources we are unable to determine whether this is a fluctuation due to insufficient statistics (our choice of parameters maximised statistical fluctuations, which may in retrospect not have been optimal), or a genuine feedback effect. The fitted value $\Phi_{\text{EoS}} = 0.1771$ emerging from the equation of state analysis presented below lies in between but closer to the ensemble generated with $L_s = 24$. We can at least conclude that even if partial quenching introduces significant systematic errors, they are fairly small.

Fig. 4 plots the condensate order parameter Φ in the $L_s \rightarrow \infty$ limit together with the original data $\bar{\Phi}_{24}$ from the RHMC production run (henceforth we drop the ∞ subscript from the extrapolated data). The extrapolation is considerably more compelling than that obtained with Shamir kernel fermions (see Fig. 4 of [12]), for which only RHMC simulations with $L_s \leq 48$ were available, and the partially quenched strategy was not employed. For the smallest mass $ma = 0.005$ the extrapolation doubles the size of the signal, underlining the need for a robust procedure. Close inspection of the figure reveals that small fluctuations about the trend in the original data are echoed, but *not* magnified in the extrapolated data, suggesting that if needed further accuracy should be attainable in a future simulation with enhanced statistics.

3.2 Equation of State

On the basis that there is a continuous U(2)-symmetry breaking phase transition at some $(\beta_c, m = 0)$, we proceed on the assumption that there is a universal scaling function \mathcal{F} applicable in the vicinity satisfying

$$m = \Phi^\delta \mathcal{F}((\beta - \beta_c)\Phi^{-1/\beta_m}), \quad (10)$$

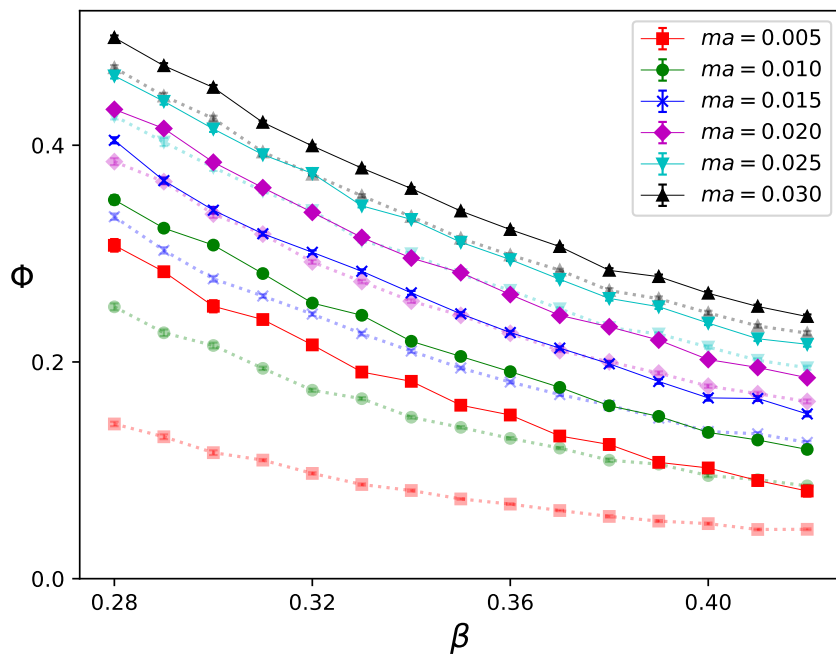


Figure 4: Bilinear condensate $\Phi(\beta, m)$ from original unitary simulation on $L_s = 24$ (faint symbols, dotted lines), and extrapolated $L_s \rightarrow \infty$ (bold symbols, full lines).

where δ, β_m are *critical exponents* characterising the universality class of the transition. For the simplest non-trivial case of a linear scaling function we obtain the following equation of state Ansatz:

$$m = A(\beta - \beta_c)\Phi^{\delta-1/\beta_m} + B\Phi^\delta, \quad (11)$$

with 5 fitting parameters. Fig. 5 shows a least squares fit to the entire dataset using

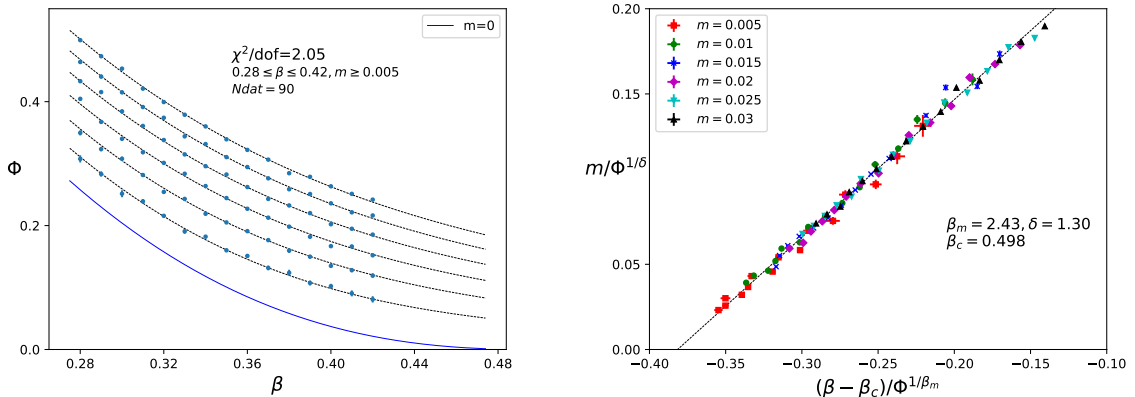


Figure 5: (Left) Least-squares fit to the equation of state (11) using all 90 data points, with the solid curve showing the $m = 0$ limit; (Right) Data collapse demonstrating the near-linear nature of the scaling function \mathcal{F} .

(11), yielding $\chi^2/\text{dof} \simeq 2$, which is modest for a global fit of this nature. The fit predicts a critical $\beta_c = 0.499(15)$, lying well outside the coupling range explored in the simulation, so that all our datapoints lie in the symmetry-broken phase. The relatively large fitted value for the exponent $\beta_m = 2.43(15) \gg 1$ results in convex constant- m curves approaching the $\Phi = 0$ axis with positive curvature. The right panel of Fig. 5 replots the data to demonstrate the validity of the linear approximation for \mathcal{F} . The negative values along the horizontal axis underline that all data lie in the broken phase. While there is some scatter around the trend line, there is no sign of any systematic departures. Our quoted values for the critical parameters are thus

$$\beta_c = 0.498(15); \quad \beta_m = 2.43(15); \quad \delta = 1.300(36). \quad (12)$$

The fit is remarkably stable; we have checked that omitting $\bar{\Phi}_{24}$ data from the extrapolation, or data with $\beta < 0.30$, $\beta > 0.40$ or $ma > 0.025$ from the fit makes negligible difference either to the quality of the fit or the fitted values, which vary well within the errors quoted in (12). Omitting $\bar{\Phi}_{120}$ from the extrapolation, which increases the size of the errors for the lightest mass $ma = 0.005$, or equivalently omitting $ma = 0.005$ data from the fit altogether does significantly alter the fit to $\beta_c = 0.453(18)$, $\beta_m = 2.06(16)$, $\delta = 1.429(49)$ with $\chi^2/\text{dof} = 2.2$. These data could conceivably be the most susceptible

to finite-volume effects not considered in this study; accordingly we take these values as conservative lower (upper) bounds for the exponents β_m (δ).

Finally, we apply hyperscaling relations to deduce the value of further exponents, defined below in Sec. 4. Hyperscaling for a critical system in d dimensions is derived under the assumption that there is a single physically-relevant scale, the correlation length ξ :

$$\delta = \frac{d+2-\eta}{d-2+\eta}; \quad \nu = \frac{1}{d}(2\beta_m + \gamma) = \frac{1}{d}(2\beta_m\delta - \gamma). \quad (13)$$

The system (13) together with the scaling relation $\gamma = \nu(2 - \eta)$ and (12) yields the accompanying predictions

$$\eta = 1.61(4); \quad \nu = 1.86(13); \quad \gamma = 0.73(9). \quad (14)$$

3.3 Susceptibility

The susceptibility associated with the fluctuating order parameter Φ is defined by

$$\chi_\ell = -\frac{\partial^2 f}{\partial m^2} = \frac{\partial \Phi}{\partial m} = V \left(\langle \Phi^2 \rangle - \langle \Phi \rangle^2 \right), \quad (15)$$

where f is the system's free energy divided by spacetime volume V . The mean square quantity $\langle \Phi^2 \rangle$ is estimated using the same noise vectors as the order parameter, retaining only off-diagonal correlations to avoid contamination from connected fermion-line contributions. χ_ℓ is an intensive quantity which may diverge near a critical point.

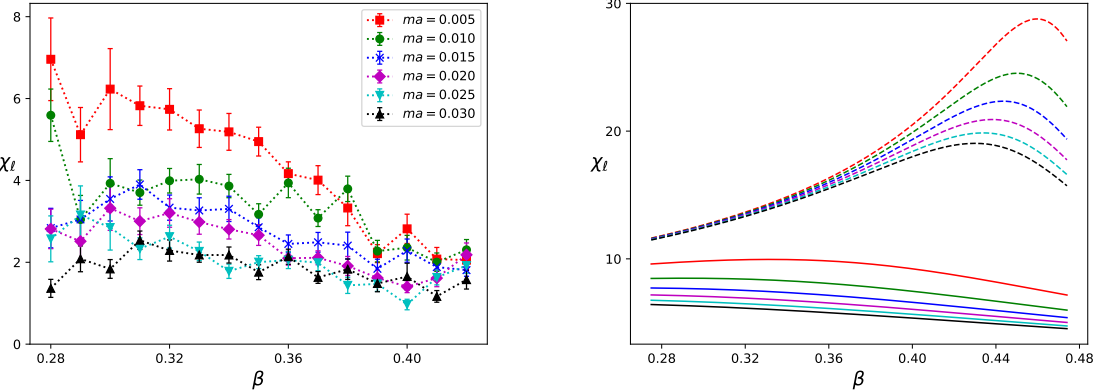


Figure 6: (Left) Susceptibility χ_ℓ estimated from the $\bar{\Phi}_{120}$ dataset; (Right) χ_ℓ derived from the fitted equation of state (11) for the fitted values m (full) and for $m \times 10^{-2}$ (dashed).

Experience with simulating the 2+1d Gross-Neveu model using domain wall fermions [10] suggests the $L_s \rightarrow \infty$ extrapolation is much more challenging for the susceptibility than for the order parameter, and the procedure followed in Sec. 3.1 yields results which are

too noisy to be useful. Accordingly Fig. 6 shows χ_ℓ estimated using measurements with fixed $L_s = 120$, together with an analytic estimate extracted from the fitted equation of state (11) using the definition (15). For these parameters the expected critical peak is rather shallow and considerably displaced to a coupling stronger than the critical $\beta_c \simeq 0.5$. The right panel of Fig. 6 suggests that bare masses $ma \sim O(10^{-4})$ would be needed in order to see a susceptibility peak develop as $\beta \rightarrow \beta_c$. The qualitative features of the analytic prediction are to some extent reproduced by the simulation data, which displays large fluctuations between independent datapoints consistent with the size of the statistical errors, and the order of magnitude of the signal is comparable, but a quantitative comparison is hardly possible. It should be noted though, that previous attempts to calculate χ_ℓ using Shamir kernel yielded unphysical results having an inverted mass hierarchy (see Fig. 9 of [12]). Fig. 15 represents a considerable improvement, strengthening our confidence that the partially quenched strategy yields physically credible results.

4 Schwinger-Dyson Interlude

Here we follow the approach to the non-perturbative modelling of the $U(2N)$ symmetry breaking introduced by Itoh *et al* [2] who derived results in the strong coupling limit $g^2 \rightarrow \infty$, and subsequently refined by Sugiura [4] who generalised to finite g^2 . They consider an N -flavor Thirring model coupled to a Stückelberg scalar field ϕ , which permits the identification of a “hidden local symmetry” $\phi(x) \mapsto \phi(x) + \alpha(x)$, with the auxiliary A_μ effectively acting as a $U(1)$ gauge field. The gauge choice $\phi \equiv 0$ recovers the original Thirring model. Next, the full fermion inverse propagator including all quantum corrections is parametrised as

$$S^{-1}(p) = iR(p^2)\not{p} + \Sigma(p^2), \quad (16)$$

enabling a set of self-consistent Schwinger-Dyson equations (SDE) for the dressing functions R, Σ to be written. The system only closes if certain truncations are made; [2] chooses to replace the full auxiliary propagator $D_{\mu\nu}$ and fermion-auxiliary vertex Γ_μ with their forms valid in the large- N limit, namely

$$\Gamma_\mu = -i\frac{g}{\sqrt{N}}\gamma_\mu; \quad D_{\mu\nu}(p^2) \sim \frac{1}{1 - \Pi(p^2)} = \frac{1}{1 + \frac{g^2}{A_d}p^{d-2}}, \quad (17)$$

where $\Pi(p)$ is a scalar function related to the vacuum polarisation tensor and $p^{d-2} \equiv (p^2)^{(d-2)/2}$ (since the underlying $1/N$ expansion is renormalisable in a continuum $d \in (2, 4)$ of spacetime dimensions, it is helpful to leave d as a parameter). Finally, the hidden local symmetry is exploited to define a non-local gauge fixing functional in which A_μ and ϕ decouple and $R(p^2) \equiv 1$, in which case the system reduces to a single integral equation for the self-energy Σ :

$$\Sigma(p) = m + \frac{N_c(d)}{4N} \int_{\mu^{d-2}}^1 dq^{d-2} \Sigma(q) \min \left\{ \left(p^{d-2} + \frac{F_d}{g^2} \right)^{-1}, \left(q^{d-2} + \frac{F_d}{g^2} \right)^{-1} \right\}, \quad (18)$$

where we have introduced a bare mass m and an IR cutoff-scale μ which will eventually be interpreted as an inverse correlation length. All dimensionful quantities $\Sigma, p, q, m, \mu, g^2$ in (18) are defined in cutoff units, so that the UV limit of the momentum integral is unity. For $d = 3$ the dimensionless constants $A_d, N_c(d), F_d$ have values

$$A_3 = 8; \quad N_c(3) = \frac{128}{3\pi^2}; \quad F_3 = 6. \quad (19)$$

The full derivation of (18), valid for finite $g^2 \gg 1$, is given in [4]; it requires expanding the gauge-fixing condition consistently to $O(g^{-2})$ and making a simplified *Ansatz* for the polar angular integration which is supported by a numerical check. Another important simplification is that $\text{tr}S_F \propto \Sigma/(q^2 + \Sigma^2)$ in the integrand is replaced by the linearised form Σ/q^2 valid for small departures from the trivial solution $\Sigma = 0$. It is now possible to recast (18) as a second-order differential equation

$$\left[\left(x + \frac{F_d}{g^2} \right)^2 \Sigma'(x) \right]' = -\frac{N_c}{4N} \Sigma(x), \quad (20)$$

with $x \equiv p^{d-2}$, supplemented by the boundary conditions

$$\Sigma'(p = \mu) = 0 \quad (\text{IR}) \quad (21)$$

$$\left. \left[\left(x + \frac{F_d}{g^2} \right) \Sigma \right]' \right|_{x=1} = m \quad (\text{UV}). \quad (22)$$

The solution to (20) is

$$\Sigma(x) = \frac{\mu}{\sin\left(\frac{\omega\varphi}{2}\right)} \left(\frac{\sigma + f}{x + f} \right)^{\frac{1}{2}} \sin \left\{ \frac{\omega}{2} \left[\ln \frac{x + f}{\sigma + f} + \varphi \right] \right\}, \quad (23)$$

with $\sigma = \mu^{d-2}$, $f = F_d/g^2$, and

$$\omega = \sqrt{\frac{N_c}{N} - 1}; \quad \varphi = \frac{2}{\omega} \tan^{-1} \omega. \quad (24)$$

For $N = 1$ relevant for the current study $\omega \simeq 1.823, \varphi \simeq 1.173$. The UV boundary condition (22) becomes

$$m = \frac{\mu(1 + \omega^2)^{\frac{1}{2}}}{2 \sin\left(\frac{\omega\varphi}{2}\right)} \left(\frac{\sigma + f}{1 + f} \right)^{\frac{1}{2}} \sin \left\{ \frac{\omega}{2} \left[\ln \frac{1 + f}{\sigma + f} + 2\varphi \right] \right\}. \quad (25)$$

Finally use the relation for the order parameter

$$\frac{G_d}{N(1 + f)^2} \langle \bar{\psi} \psi \rangle = -\Sigma'(x = 1) \quad (26)$$

with $G_3 = \frac{16}{3}$ to find

$$\frac{G_d}{N} \langle \bar{\psi} \psi \rangle = \frac{\mu(1 + \omega^2)^{\frac{1}{2}}}{2 \sin\left(\frac{\omega\varphi}{2}\right)} \sqrt{(\sigma + f)(1 + f)} \sin\left\{\frac{\omega}{2} \ln \frac{1 + f}{\sigma + f}\right\}. \quad (27)$$

To proceed we solve the UV boundary condition (25) for $m = 0$ by finding a nodeless zero of the sine function, corresponding to the ground state:

$$\left(\frac{\mu}{\Lambda}\right)^{d-2} = (1 + f)e^{2\varphi} \exp\left(-\frac{2\pi}{\sqrt{\frac{N_c}{N} - 1}}\right) - f \sim \xi^{2-d}, \quad (28)$$

where we have restored explicit UV cutoff Λ -dependence to stress the relation with the correlation length ξ . The critical system has $\mu/\Lambda \rightarrow 0$ enabling the identification of a critical coupling g_c^2 :

$$\frac{g_c^2}{\Lambda^{d-2}} = F_d \left(\exp\left[\frac{2\pi}{\omega} - 2\varphi\right] - 1 \right), \quad (29)$$

such that the non-trivial solution (23) is the physical one for $N < N_c, g^2 > g_c^2(N)$. The critical coupling g_c^2 diverges as $\omega \rightarrow 0, N \rightarrow N_{c-}$. For $d = 3, N = 1$ we have $g_c^2/\Lambda \simeq 12.04$.

To extract further critical information we use the order parameter (27) [18]. Away from strong coupling in the critical regime $\sigma \ll f$ and using dimensional analysis we deduce $\langle \bar{\psi} \psi \rangle \propto \mu \Lambda^{d-2}$; however, for $N \sim N_c$ $\sigma \gg f$ and $\langle \bar{\psi} \psi \rangle \propto \mu^{\frac{d}{2}} \Lambda^{\frac{d}{2}-1}$. The cutoff dependence yields the anomalous dimension of the composite $\bar{\psi} \psi$:

$$\gamma_{\bar{\psi} \psi} = \frac{d \ln \langle \bar{\psi} \psi \rangle}{d \ln \Lambda} = \begin{cases} \frac{d}{2} - 1; & \text{strong coupling} \\ d - 2; & \text{otherwise.} \end{cases} \quad (30)$$

In turn this is related to the critical exponent η governing critical correlations of the order parameter fluctuations $\langle \bar{\psi} \psi(0) \bar{\psi} \psi(r) \rangle \propto 1/r^{d-2+\eta}$ [19]:

$$\eta = d - 2\gamma_{\bar{\psi} \psi} = \begin{cases} 2; & \text{strong coupling} \\ 4 - d; & \text{otherwise.} \end{cases} \quad (31)$$

Finally, hyperscaling (13) enables the extraction of the exponent δ :

$$\delta = \frac{d + 2 - \eta}{d - 2 + \eta} = \begin{cases} 1; & \text{strong coupling} \\ d - 1; & \text{otherwise.} \end{cases} \quad (32)$$

It is important to stress that the limits $N \rightarrow N_{c-}, g^2 \rightarrow g_{c+}^2$ do not commute; in this super-critical regime the SDE critical exponents depend on the order of limits and do not smoothly vary between the two cases set out in (31,32), in contrast to the sub-critical regime of the gauged NJL model in $d = 4$ explored in [20].

Away from the strong coupling limit it is possible to extract exponents by more direct means. The UV boundary condition (28) can be rearranged to read

$$\xi = \left(\frac{1 + f_c}{F_d} \right)^{\frac{1}{d-2}} |t|^{-\frac{1}{d-2}} \quad (33)$$

with $t = g^{-2} - g_c^{-2}$, whence we identify the correlation length exponent

$$\nu = \frac{1}{d-2}. \quad (34)$$

Next, rewrite (25) with $m > 0$:

$$\frac{m}{\mu} = Q \sin(\pi - \varepsilon) \approx Q\varepsilon \quad (35)$$

where we assume $\varepsilon \ll 1$, so that $e^{2\varepsilon/\omega} \simeq 1 + \frac{2\varepsilon}{\omega}$ and

$$\sigma = -\frac{F_d}{1 + f_c} t + \frac{2\varepsilon}{\omega} \frac{1 + f}{1 + f_c^{-1}} \Rightarrow m = \tilde{A}t\mu + \tilde{B}\mu^{d-1} = At\Phi + B\Phi^{d-1}, \quad (36)$$

where the final step applies the scaling $\langle \bar{\psi}\psi \rangle \propto \mu$ valid away from strong coupling. Comparison with the trial equation of state (11) recovers $\delta = d - 1$ and the additional prediction

$$\beta_m = \frac{1}{d-2}. \quad (37)$$

Finally the order parameter susceptibility

$$\chi_\ell = \frac{\partial \Phi}{\partial m} \Big|_{m=0} = \frac{1}{A(d-2)|t|} \propto |t|^{-\gamma} \Rightarrow \gamma = 1. \quad (38)$$

The exponents derived for g^2 finite coincide with those of the $d = 3$ Gross-Neveu (GN) model in the large- N limit (see eg. [19]).

5 Discussion

The results reported here show compelling evidence for a U(2) symmetry-breaking transition in the 3d $N = 1$ Thirring model at large but finite interaction strength. The equation of state fits are stable over the whole parameter range studied, yielding values for two critical exponents δ and β_m , which enables derivation of all others related to the order parameter assuming the validity of hyperscaling. The key improvement over earlier studies is much better control over the $L_s \rightarrow \infty$ limit required for U(2) symmetry restoration in the DWF formulation. Before examining the implications we need to specify some important caveats. Firstly, our partially-quenched procedure, extrapolating measurements for varying L_s on auxiliary field configurations obtained with fixed finite

$L_s = 24$, is an uncontrolled and non-unitary approximation. As presented in Sec. 3.1, Table 1, a calibration simulation on $L_s = 32$ suggests quenching effects are small, but with the limited data available at this stage a small but statistically-significant effect cannot be ruled out. Secondly, all results are obtained on a fixed spacetime volume 16^3 ; while previous studies suggest finite volume corrections are small for similar models, because the current system looks so different we cannot rule out important effects without more extensive study. Finally, comparison of the left and right panels of Fig. 2 shows that as $L_s \rightarrow \infty$ the residual δ_h approaches zero more slowly than the condensate $\bar{\Phi}(L_s)$ approaches its extrapolated values Φ_∞ , implying that U(2) symmetry may still not be manifest even for the extrapolated system we have analysed. This issue also requires further study.

The system is “different” because the fitted values in (12) give robust evidence for $\delta < 2$, $\beta_m > 2$, in marked contrast to all other studies of the 3d Thirring model using lattice field theory, which yield $\delta > 2$, $\beta_m < 1$. Correspondingly, critical correlations appear to be governed by $\eta > 1$, whereas previous studies have yielded $\eta < 1$. For a review see [8], and for a discussion of $N > 1$ with staggered fermions see [18]. The equation of state plotted in Fig. 5 has everywhere convex fit curves, resulting in an unusually large fitted uncertainty for the critical coupling β_c . The susceptibility in Fig. 6 shows a shallow peak at $\beta \approx 0.3$ only at the lightest mass $ma = 0.005$, well displaced to the strong-coupling side of β_c . The fitted equation of state suggests fermion masses perhaps a hundred times smaller will be needed before a sizeable peak centred close to β_c emerges. It is safe to state, therefore, that compared to previous lattice work the current study reveals a new and radically different account of the Thirring model.

One way of articulating the difference is to note that for the first time lattice field theory simulations reveal a picture qualitatively similar to that emerging from self-consistent solution of truncated Schwinger-Dyson equations, in the sense that $\delta < 2$, $\eta > 1$, $\beta_m > 2$. Sec. 4 reviewed an analytic approach to Thirring criticality based on SDE solutions. Rather unsatisfactorily, the answers depend on the order of limits: if the strong-coupling limit is taken first, there is an essentially singular scaling (28) of ξ as $N \rightarrow N_{c-}$, with $\delta = 1$, $\eta = 2$ but other exponents undefined. If by contrast we study $g^2 \rightarrow g_c^2$ at fixed $N < N_c$, then $\delta = 2$, $\eta = \beta = \nu = \gamma = 1$. While the exponents predicted in this case coincide with those of the large- N GN model, they show no further dependence on N , in marked contrast to GN models where exponents can be calculated systematically in a large- N expansion [19].

How credible is this? Perhaps N -independence is a consequence of the vanishing of higher-order corrections to the leading-order vacuum polarisation contribution to the auxiliary propagator, which has been argued to be essential for the $1/N$ renormalisability of the model [21]. Alternatively, perhaps the N -independence is an artefact of the SDE truncations applied, and a more complete solution might reveal a scenario qualitatively similar to [20], with exponents varying smoothly along the critical line in the (g^{-2}, N) plane, ending in an essential singularity at $(0, N_c)$ where $\delta = 1$, $\eta = 2$ and β, ν diverge. The fitted values (12) seem tantalisingly to favour this possibility, and strongly motivate a renewed simulation campaign with $N = 2$, first studied in [11].

Data Availability

The simulation data generated for the analysis reported in Sec. 3 are freely available at [22], along with links to the production source code.

Acknowledgements

This work used the DiRAC Data Intensive service (CSD3) at the University of Cambridge managed by the University of Cambridge University Information Services, and the DiRAC Data Intensive service (DIAL 2.5) at the University of Leicester, managed by the University of Leicester Research Computing Service, each on behalf of the STFC DiRAC HPC Facility [23]. The DiRAC component of CSD3 at Cambridge, and the DiRAC service at Leicester were funded by BEIS, UKRI and STFC capital funding and STFC operations grants. Additional time on CSD3 was supported by the UKRI *Access to HPC* scheme. DiRAC is part of the UKRI Digital Research Infrastructure. We are grateful for the help given by Connor Aird and Jamie Quinn of UCL’s Centre for Advanced Research Computing funded by DiRAC, and to Chris Allton and Ryan Bignell of FASTSUM and Johann Ostmeyer for their support. The work of JW was supported by an EPSRC studentship.

References

- [1] M. Gomes, R.S. Mendes, R.F. Ribeiro and A.J. da Silva, Phys. Rev. D **43** (1991), 3516-3523 doi:10.1103/PhysRevD.43.3516
- [2] T. Itoh, Y. Kim, M. Sugiura and K. Yamawaki, Prog. Theor. Phys. **93**, 417 (1995) doi:10.1143/PTP.93.417
- [3] T. Ebihara, T. Iizuka, K.I. Kondo and E. Tanaka, Nucl. Phys. B **434** (1995), 85-108 doi:10.1016/0550-3213(94)00457-P
- [4] M. Sugiura, Prog. Theor. Phys. **97** (1997) 311 doi:10.1143/PTP.97.311
- [5] H. Gies and L. Janssen, Phys. Rev. D **82** (2010) 085018 doi:10.1103/PhysRevD.82.085018
- [6] L. Janssen and H. Gies, Phys. Rev. D **86** (2012) 105007 doi:10.1103/PhysRevD.86.105007
- [7] F. Gehring, H. Gies and L. Janssen, Phys. Rev. D **92** (2015) 085046 doi:10.1103/PhysRevD.92.085046
- [8] S. Hands, *Peter Suranyi 87th Birthday Festschrift*, pp. 217-236 (2022) (World Scientific) doi:10.1142/9789811262357_0013 [arXiv:2105.09643 [hep-lat]].

- [9] A.W. Wipf and J.J. Lenz, *Symmetry* **14** (2022) no.2, 333 doi:10.3390/sym14020333
- [10] S. Hands, *JHEP* **1611** (2016) 015 doi:10.1007/JHEP11(2016)015
- [11] S. Hands, *Phys. Rev. D* **99** (2019) no.3, 034504 doi:10.1103/PhysRevD.99.034504
- [12] S. Hands, M. Mesiti and J. Worthy, *Phys. Rev. D* **102** (2020) no.9, 094502 doi:10.1103/PhysRevD.102.094502
- [13] S. Hands and J. Ostmeyer, *Phys. Rev. D* **107** (2023) no.1, 014504 doi:10.1103/PhysRevD.107.014504
- [14] S. Hands, *JHEP* **1509** (2015) 047 doi:10.1007/JHEP09(2015)047
- [15] S. Hands, *Phys. Lett. B* **754** (2016) 264 doi:10.1016/j.physletb.2016.01.037
- [16] J. Worthy and S. Hands, *Int. J. Mod. Phys. C* **36** (2025) 25500020 doi:10.1142/S0129183125500020 [arXiv:2410.04077 [hep-lat]].
- [17] S. Hands and J. Worthy, PoS **LATTICE2023** (2024), 338 doi:10.22323/1.453.0338
- [18] S. Christofi, S. Hands and C. Strouthos, *Phys. Rev. D* **75** (2007), 101701 doi:10.1103/PhysRevD.75.101701
- [19] S. Hands, A. Kocić and J.B. Kogut, *Annals Phys.* **224** (1993), 29-89 doi:10.1006/aphy.1993.1039
- [20] A. Kocić, S. Hands, J.B. Kogut and E. Dagotto, *Nucl. Phys. B* **347** (1990), 217-242 doi:10.1016/0550-3213(90)90558-U
- [21] S. Hands, *Phys. Rev. D* **51** (1995) 5816 doi:10.1103/PhysRevD.51.5816
- [22] S. Hands and J. Worthy, doi:10.17638/datacat.liverpool.ac.uk/3006
- [23] www.dirac.ac.uk